

Model and Simulation of an SMA Enhanced Lip Seal

Rui Qiao, Xiujie Gao, and L. Catherine Brinson

(Submitted June 18, 2010; in revised form February 14, 2011)

The feasibility of using SMA wires to improve the seal effectiveness has been studied experimentally and numerically. In this article, we present only the numerical study of simulating the thermo-mechanical behavior for an SMA enhanced lip seal, leaving the test setup and results in the experimental counterpart. A pseudo 3D SMA model, considering 1D SMA behavior in the major loading direction and elastic response in other directions, was used to capture the thermo-mechanical behavior of SMA wires. The model was then implemented into ABAQUS using the user-defined material subroutine to inherit most features of the commercial finite element package. Two-way shape memory effect was also considered since the SMA material exhibits strong two-way effects. An axisymmetric finite element model was constructed to simulate a seal mounting on a shaft and the sealing pressure was calculated for both the regular seal and the SMA enhanced seal. Finally, the result was qualitatively compared with the experimental observation.

Keywords ABAQUS, lip seal, pseudo 3D, shape memory alloys, SMA model, two-way shape memory effect, TWSME, UMAT

1. Introduction

Lip seals are known to potentially have sealing issues due to softening of polymer materials at high temperature. The reducing of contact pressure as temperature increasing can be a severe problem because it may cause the fluid leaking during operation and impact the function of the device. One example is the application of lip seals in the rheological fluid-based real-time controllable damper presented in the experimental counterpart of this article (Ref 1). As observed in the experiment (Ref 1), the leaking of magneto-rheological (MR) fluids from housing may cause the damper working improperly. Therefore, seals that have capability to adapt the change of temperature are very desirable. As smart materials, shape memory alloys (SMAs) have the capability to change their shape corresponding to the temperature in the environment, due to the phase transformation in the material. Particularly, a large recovery force can be produced by SMAs during the transformation if they are restrained. Hence, if mounting SMA wires or ribbons on a seal, it is expected that the wires or ribbons will

produce additional constraint on the seal at high temperatures and reduce the temperature induced variation of sealing pressure.

A numerical simulation can provide a quick evaluation of the feasibility of using SMA wires to improve the seal effectiveness, and also an effective tool for design and optimization of the device. In previous study (Ref 2), a rigorous one-dimensional shape memory alloy constitutive model has been implemented into ABAQUS by developing a user element subroutine, which provides a method to simulate the thermo-mechanical behavior of structures with one-dimensional SMA components. However, the one dimensionality of the model restricts its application for this study in which the contact between the SMA wire/ribbon and the seal needs to be considered. Therefore, a model with the capability to capture simple spatial responses of SMA components is necessary for this study. Considering an SMA wire, it is reasonable to assume that the axial stress is much higher than stresses in other directions and the shape memory behavior is mainly exhibited in the axial direction. Therefore, a pseudo 3D constitutive model was developed, which uses the one-dimensional Brinson model (Ref 3) to simulate the thermo-mechanical behavior of an SMA in the axial direction and assumes elastic response in other directions.

The model was implemented into ABAQUS using a user-defined material subroutine (UMAT) so that it inherits most features of the commercial finite element package including support for most continuum elements, contact analysis, compatibility with ABAQUS CAE, etc. Two-way shape memory effect (TWSME) was also considered in this study because the SMA wires used in the experiment exhibit such behavior. A simple but effective approach to simulate the TWSME is to shift the phase diagram to the negative stress region.

An axisymmetric finite element model, as illustrated in Fig. 1, was constructed to simulate the thermo-mechanical behavior of the SMA enhanced seal (Ref 1). The simulation was performed in ABAQUS Standard with the UMAT of the pseudo 3D SMA model presented in this article. Due to limitation of the measurement system and insufficient material properties, the predicted results are qualitatively compared with

This article is an invited paper selected from presentations at Shape Memory and Superelastic Technologies 2010, held May 16-20, 2010, in Pacific Grove, California, and has been expanded from the original presentation.

Rui Qiao, BD Medical Research & Development, 9450 South State Street, Sandy, UT 84070; **Xiujie Gao**, General Motors R&D, MC 480-106-256, 30500 Mound Rd, Warren, MI 48090; **L. Catherine Brinson**, Department of Mechanical Engineering, Northwestern University, Evanston, IL 60208; and Department of Materials Science & Engineering, Northwestern University, Evanston, IL 60208. Contact e-mail: jay.gao@gmail.com.

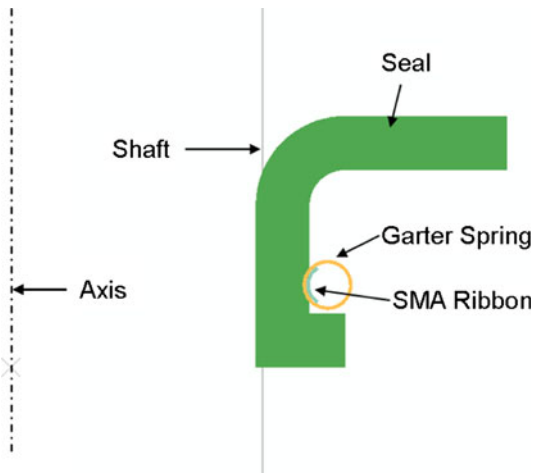


Fig. 1 Axisymmetric model of the SMA enhanced seal. The geometries of seal and shaft are the same as the prototype built for the experiment

the experimental results. This article focuses on the numerical modeling of the sealing performance of the SMA enhanced seal and comparison of the analysis results with the experimental measurements. Readers can refer to the experimental part (Ref 1) for the test setup and observations.

This article is organized as follows. Section 2 describes the mathematical expression of the pseudo 3D SMA model, followed by the implementation into ABAQUS via a user-defined material subroutine and how the two-way shape memory effects are considered. The finite element simulation of SMA enhanced seal is described in section 4. Finally, section 5 presents the conclusions of this study.

2. SMA Constitutive Law and Transformation Kinetics

Since SMA wires and ribbons in smart structure applications are usually subjected to a variety of thermal and mechanical load profiles, including cyclic loading, partial forward and reverse transformation, and simultaneous changes in load and temperature, the constitutive law and kinetics chosen to be implemented must be robust and able to capture complex thermo-mechanical cycles. In this section, we first briefly review the constitutive law developed by Brinson (Ref 3). Then, we present the extension of the 1D model to a pseudo 3D which is capable of satisfying the basic usage in 3D structures.

2.1 1D Brinson Model

One important feature of the 1D Brinson model is to distinguish between the self-accommodated (twinned) and oriented (detwinned) martensite in the material. Self accommodated martensite, ξ_t , is temperature-induced with no associated macroscopic strain, while oriented martensite, ξ_o , has a crystal structure that has been preferentially oriented by the applied load and is accompanied by a macroscopic strain. The total martensite volume fraction is composed of these two components:

$$\xi = \xi_t + \xi_o \quad (\text{Eq 1})$$

The use of these two martensite internal variables allows this model to capture the full range of SMA behavior, including shape memory effect and pseudoelasticity.

The constitutive law of one-dimensional shape memory alloys can be written as (Ref 3, 4):

$$\sigma = E(\xi)(\varepsilon - e_L \xi_o) + \Theta(T - T_0) \quad (\text{Eq 2})$$

where E and Θ are the modulus and thermal coefficient of expansion of the material, respectively. e_L is the maximum residual strain for the given SMA material. T_0 is the reference temperature at which thermal strain is defined to be zero. Here, $E(\xi)$ is taken to be a function of the martensite fraction of the material:

$$E(\xi) = \xi E_m + (1 - \xi) E_a \quad (\text{Eq 3})$$

where E_m is the modulus value for the SMA as 100% martensite and E_a is the modulus value for the SMA as 100% austenite. The rule of mixtures is commonly used to approximate the material property of martensite and austenite mixtures. If the approximation is done on the elastic constant like Eq 3, it assumes an iso-strain condition. However, if it is used on the compliance constant, then it assumes an iso-stress condition (Ref 5). In 1D case, the iso-strain approximation behaves like a parallel model, and the iso-stress approximation assumes a series model. They will yield the same result when the material is either pure martensite or austenite. They will yield different results otherwise but the maximum difference is only about 15% (Ref 6). Since the real mixture of martensite and austenite is neither parallel nor series, the choice is by the author and convenience of formulation.

If the thermal strain component is neglected (since it is orders of magnitude smaller than the transformation strain under moderate temperature changes), the constitutive law is simplified further to

$$\sigma = (\xi E_m + (1 - \xi) E_a)(\varepsilon - e_L \xi_o) \quad (\text{Eq 4})$$

It is worth noting that the stress in Eq 14 in a later section refers to the second Piola-Kirchhoff stress. However, for our application (small deformation and no rigid body motion), the difference between the Cauchy stress and the second Piola-Kirchhoff stress is negligible. Therefore, for consistency and simplicity, all stress refers to the Cauchy stress in the rest of this article.

2.2 Pseudo-3D Extension

For many applications of one-dimensional SMA components, such as SMA wires and ribbons, the SMA elements are primarily loaded axially and the axial stress can be several orders of magnitude higher than the stresses in other directions. Moreover, the axial deformation is much more significant in comparison with the radial change in those applications. Therefore, it is reasonable to consider the shape memory behavior only in the axial direction and assume elasticity in other directions.

Assuming the phase transformation exists only in the loading axis, the mathematic expression of the material constitutive law can be written as:

$$\sigma_{ij} = \lambda e_{kk} \delta_{ij} + 2\mu e_{ij} - \lambda \xi_o e_L \delta_{ij} - 2\mu \xi_o \delta_{i1} \delta_{j1} \quad (\text{Eq 5})$$

where λ and μ are the Lamé constants and the material is assumed isotropic except that the “1” direction is the primary

loading axis along which the SMA behavior persists. The equation above can be derived by the following procedure:

With application of only σ_{11} , the strain in the loading direction can be determined from the 1D SMA constitutive law and the other components from Poisson's effect.

$$e_{11} = \frac{\sigma_{11}}{E} + \xi_0 e_L \quad (\text{Eq 6})$$

$$e_{22} = e_{33} = -\frac{\nu}{E} \sigma_{11}$$

With application of only σ_{22} , the strain field is given by:

$$e_{22} = \frac{\sigma_{22}}{E} \quad (\text{Eq 7})$$

$$e_{11} = e_{33} = -\frac{\nu}{E} \sigma_{22}$$

With application of only σ_{33} , the equations are similar to above, interchanging subscripts 2 and 3. Superposing all three tensile stresses and three shear stresses and assuming isotropic elastic in shear stress, we can obtain the strain-stress relation:

$$e_{ij} = \sigma_{ij} \frac{(1+\nu)}{E} - \frac{\nu}{E} \sigma_{kk} \delta_{ij} + \xi_0 e_L \delta_{i1} \delta_{j1} \quad (\text{Eq 8})$$

The general constitutive laws are obtained by inverting the equation above. If thermal expansion is considered in the SMA material, the thermal stress is added to this equation*:

$$\sigma_{ij} = \lambda e_{kk} \delta_{ij} + 2\mu e_{ij} - \lambda \xi_0 e_L \delta_{ij} - 2\mu \xi_0 \delta_{i1} \delta_{j1} - (3\lambda + 2\mu)\alpha(T - T_0)\delta_{ij} \quad (\text{Eq 9})$$

where T_0 is the reference temperature at which the thermal strain is defined to be zero and α is the thermal expansion coefficient of the material calculated by rule-of-mixture:

$$\alpha = \alpha_m \xi + \alpha_a (1 - \xi) \quad (\text{Eq 10})$$

where α_m is the thermal expansion coefficient of SMA at martensite phase and α_a is that of SMA at austenite phase.

2.3 Transformation Kinetics

The transformation kinetic equations relate the evolution of the martensite volume fraction with stress and temperature. The choice of transformation kinetics is critical to ensure robust performance of the overall constitutive response of the SMA material due to the history dependence of the materials transformation behavior. In this article, we adopt a phase diagram-based kinetic description which was first rigorously derived by Bekker and Brinson and then fully extended to all regions (Ref 2, 7). A typical stress-temperature phase diagram shown in Fig. 2 is used in the kinetics to track the SMA phase transformation. This diagram is composed of transformation/reorientation zones [A] (martensite to austenite), [t] (austenite to self-accommodated (twinned) martensite), [M] (austenite and/or self-accommodated martensite to oriented martensite), and [o] (self-accommodated martensite to oriented (detwinned) martensite). The overlapping zone of [o] and [t] is denoted as [o, t]. The other regions are either dead zones in which no transformation or orientation occurs or the plastic region. The mathematical derivation of the transformation kinetics is omitted in this article and readers can refer to cited literature for details. Instead, the mathematical expressions describing the

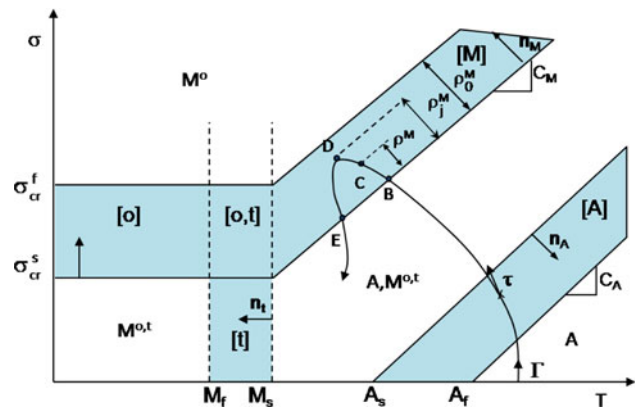


Fig. 2 A typical one-dimensional phase diagram of shape memory alloys. The shaded regions are the transformation strips, while other regions are “dead zones” where no change in martensite fractions occurs. Γ is an arbitrary loading path with points B-E denoted on it, where B and E are the entrance and exit points, respectively; C is the “current point;” D is a switching point where transformation stops

martensite fraction evolution in different zones are summarized as follows:

The martensite fraction evolution in the zones for forward (martensite to austenite) and reverse transformation (austenite to martensite) can be written as

$$\xi = F^A = \xi_j f^A(Z^A) \quad (\text{Eq 11})$$

where the subscript j represents the switching point and the superscripts A refers to austenite. f^A is the transformation function with values being interpolated between 0 and 1 (Ref 6, 8-12). Given the cosine function, the transformation functions are defined as

$$f^A(Z^i) = 1 - \frac{1}{2} [1 - \cos(\pi Z^i)] \quad (\text{Eq 12})$$

where Z^i is a distance ratio in zone i with reference to the last transformation switching point, j . Z^i is a function of temperature and stress and can be calculated by equation of

$$Z^i = \frac{\rho^i - \rho_j^i}{\rho_0^i - \rho_j^i} = \frac{n_1^i(T - T_{in}^i) + n_2^i(\sigma - \sigma_{in}^i) - n_1^i(T_j - T_{in}^i) - n_2^i(\sigma_j - \sigma_{in}^i)}{n_1^i(T_{out}^i - T_{in}^i) + n_2^i(\sigma_{out}^i - \sigma_{in}^i) - n_1^i(T_j - T_{in}^i) - n_2^i(\sigma_j - \sigma_{in}^i)} = \frac{n_1^i(T - T_j) + n_2^i(\sigma - \sigma_j)}{n_1^i(T_{out}^i - T_j) + n_2^i(\sigma_{out}^i - \sigma_j)}, \quad i = A, t, M, \text{ or } o \quad (\text{Eq 13})$$

where the parameters in different transformation zones can be found in Table 1.

3. Implementation into ABAQUS

The pseudo 3D SMA model as well as the kinetic laws discussed above has been implemented into ABAQUS using the user-defined material subroutine (UMAT) provided by the software. With assistance of this UMAT, it enables ABAQUS the capability to calculate the thermo-mechanical behaviors of structures containing SMA wires or ribbons. Moreover, the

*Note that the thermal expansion coefficient α , instead of Θ is used to calculate the thermal stress in remainder of this article.

Table 1 Entrance and exit points and normal directions for different zones

Zone	$(T_{in}^i, \sigma_{in}^i)$	(n_1^i, n_2^i)	$(T_{out}^i, \sigma_{out}^i)$
[A]	$(A_s, 0)$	$\frac{C_A}{\sqrt{1+C_A^2}}, \frac{-1}{\sqrt{1+C_A^2}}$	$(A_f, 0)$
[t]	$(M_s, 0)$	$-1, 0$	$(M_f, 0)$
[M]	(M_s, σ_s^{cr})	$\frac{C_M}{\sqrt{1+C_M^2}}, \frac{1}{\sqrt{1+C_M^2}}$	(M_s, σ_f^{cr})
[o]	(M_s, σ_s^{cr})	$\frac{C_d}{\sqrt{1+C_d^2}}, \frac{1}{\sqrt{1+C_d^2}}$	(M_s, σ_f^{cr})

$(T_{in}^i, \sigma_{in}^i)$ and $(T_{out}^i, \sigma_{out}^i)$ are the in and out reference points for distance calculation for the phase transformation zone i , respectively (see Fig. 2)

UMAT is compatible with ABAQUS CAE, thus inheriting most features of pre-processing and post-processing.

The linearization of the constitutive laws was conducted to obtain the material Jacobian matrix that is required by UMAT to define the constitutive behavior of the material. The last switching point solved by the previous step is defined and stored in the program to assist in implementation (Ref 2), denoted by “swit.” It is worth noting that the Cauchy stress-temperature phase diagram is treated as a Second Piola-Kirchhoff stress-temperature phase diagram in the derivation for simplicity; since, only small displacements are involved, the difference involved is negligible.

3.1 Time Discrete and the Tangent Modulus

By taking time derivative on Eq 5, we can obtain the rate form of the constitutive laws. For the one-direction in which the shape memory behavior persists, it can be written as

$$\dot{\sigma}_{11} = (\lambda + 2\mu)\dot{e}_{11} + (\dot{\lambda} + 2\dot{\mu})e_{11} + \lambda(\dot{e}_{22} + \dot{e}_{33}) + \dot{\lambda}(e_{22} + e_{33}) - (\lambda + 2\mu)e_L\dot{\xi}_0 - (\dot{\lambda} + 2\dot{\mu})e_L\xi_0 \quad (\text{Eq 14})$$

First, we consider the material response in the transformation zone [A] in which the reverse phase transformation happens. The estimated martensite fractions are calculated using Eq 11, which is

$$\begin{aligned} \xi_0 &= \xi_0^{swit} \cdot f^A(Z^A) = \xi_0^{swit} \cdot \left[\frac{1}{2} + \frac{1}{2}\cos(\pi Z^A)\right] \\ \xi_t &= \xi_t^{swit} \cdot f^A(Z^A) = \xi_t^{swit} \cdot \left[\frac{1}{2} + \frac{1}{2}\cos(\pi Z^A)\right] \end{aligned} \quad (\text{Eq 15})$$

where Z^A is determined from Eq 13 and Table 1.

Replacing the Lamé constants* in Eq 14 by Young’s Modulus and Poisson’s ratio and utilizing Eq 3 and 15, the rate form of the constitutive equation (Eq 14) can be rewritten as

*Note that in single crystals the austenite phase is isotropic and the martensite phase is not. In polycrystals, the austenite phase may be textured or random and the martensite phase is even more complex. Since the focus is on the phase transformation which is nearly a volume free change process (Ref 13) we assume both phases are isotropic so that the elastic responses can be described using two constants. Furthermore, we assume they have the same and constant Poisson’s ratio that is independent of the martensite fraction in this article. The derivation is remarkably simplified using this approximation and the difference has little impact on the behavior in the loading direction.

$$\begin{aligned} \dot{\sigma}_{11} & \left[1 - \frac{(1-\nu)(e_{11} - \xi_0 e_L)}{(1+\nu)(1-2\nu)}(D_m - D_a)(\xi_0^{swit} + \xi_t^{swit})H_1 \right. \\ & \left. + \frac{(1-\nu)D}{(1+\nu)(1-2\nu)}e_L\xi_0^{swit}H_1 \right. \\ & \left. - \frac{\nu(e_{22} + e_{33})}{(1+\nu)(1-2\nu)}(D_m - D_a)(\xi_0^{swit} + \xi_t^{swit})H_1 \right] \\ & = (\lambda + 2\mu)\dot{e}_{11} + \lambda(\dot{e}_{22} + \dot{e}_{33}) \end{aligned} \quad (\text{Eq 16})$$

where H_1 is

$$H_1 = \sin(\pi Z^A) \cdot \frac{-\frac{1}{2}\pi n_2^A}{n_1^A(T_{out}^A - T_j) + n_2^A(\sigma_{out}^A - \sigma_j)} \quad (\text{Eq 17})$$

If multiply a time increment Δt on the both side of Eq 16, the equation becomes:

$$\begin{aligned} \Delta\sigma_{11} & \left[1 - \frac{(1-\nu)(e_{11} - \xi_0 e_L)}{(1+\nu)(1-2\nu)}(D_m - D_a)(\xi_0^{swit} + \xi_t^{swit})H_1 \right. \\ & \left. + \frac{(1-\nu)D}{(1+\nu)(1-2\nu)}e_L\xi_0^{swit}H_1 \right. \\ & \left. - \frac{\nu(e_{22} + e_{33})}{(1+\nu)(1-2\nu)}(D_m - D_a)(\xi_0^{swit} + \xi_t^{swit})H_1 \right] \\ & = (\lambda + 2\mu)\Delta e_{11} + \lambda(\Delta e_{22} + \Delta e_{33}) \end{aligned} \quad (\text{Eq 18})$$

Thus,

$$\begin{aligned} \frac{\partial\Delta\sigma_{11}}{\partial\Delta e_{11}} &= \frac{mD}{1 - H_1(H_2 + H_3)} & \frac{\partial\Delta\sigma_{11}}{\partial\Delta e_{22}} &= \frac{nD}{1 - H_1(H_2 + H_3)} \\ \frac{\partial\Delta\sigma_{11}}{\partial\Delta e_{33}} &= \frac{nD}{1 - H_1(H_2 + H_3)} \end{aligned} \quad (\text{Eq 19})$$

where

$$m = \frac{1-\nu}{(1+\nu)(1-2\nu)}, \quad n = \frac{\nu}{(1+\nu)(1-2\nu)}$$

H_1 is given by Eq 17

$$\begin{aligned} H_2 &= m(e_{11} - e_L\xi_0)(D_m - D_a)(\xi_0^{swit} + \xi_t^{swit}) - m e_L D \xi_0^{swit} \\ H_3 &= n(e_{22} + e_{33})(D_m - D_a)(\xi_0^{swit} + \xi_t^{swit}) \end{aligned} \quad (\text{Eq 20})$$

Similarly, the rate form of Eq 5 in the two-direction can be written as:

$$\begin{aligned} \dot{\sigma}_{22} &= (\lambda + 2\mu)\dot{e}_{22} + (\dot{\lambda} + 2\dot{\mu})e_{22} + \lambda(\dot{e}_{11} + \dot{e}_{33}) \\ & \quad + \dot{\lambda}(e_{11} + e_{33}) - \lambda e_L\dot{\xi}_0 - \dot{\lambda}e_L\xi_0 \end{aligned} \quad (\text{Eq 21})$$

After including the transformation kinetics and applying the same linearization procedure, we can rewrite the equation above as:

$$\begin{aligned} \Delta\sigma_{22} &= \Delta\sigma_{11} \left[(m e_{22} - n e_L \xi_0)(D_m - D_a)(\xi_0^{swit} + \xi_t^{swit})H_1 \right. \\ & \quad \left. - n D e_L \xi_0^{swit} H_1 + n(e_{11} + e_{33})(D_m - D_a)(\xi_0^{swit} + \xi_t^{swit})H_1 \right] \\ & \quad + m D \Delta e_{22} + n D (\Delta e_{11} + \Delta e_{33}) \end{aligned} \quad (\text{Eq 22})$$

Here, m and n are defined in Eq 20. Combining Eq 22 and 19, we can obtain

$$\begin{aligned} \frac{\partial\Delta\sigma_{22}}{\partial\Delta e_{11}} &= \frac{H_1(H_4 + H_5)mD}{1 - H_1(H_2 + H_3)} + nD \\ \frac{\partial\Delta\sigma_{22}}{\partial\Delta e_{22}} &= \frac{H_1(H_4 + H_5)nD}{1 - H_1(H_2 + H_3)} + mD \\ \frac{\partial\Delta\sigma_{22}}{\partial\Delta e_{33}} &= \frac{H_1(H_4 + H_5)nD}{1 - H_1(H_2 + H_3)} + nD \end{aligned} \quad (\text{Eq 23})$$

where

$$H_4 = (me_{22} - ne_L \xi_0)(D_m - D_a)(\xi_0^{\text{swit}} + \xi_t^{\text{swit}}) - nDe_L \xi_0^{\text{swit}}$$

$$H_5 = n(e_{11} + e_{33})(D_m - D_a)(\xi_0^{\text{swit}} + \xi_t^{\text{swit}}) \quad (\text{Eq 24})$$

Due to the transversal isotropic properties of the constitutive equations, we can easily obtain the material response in the three-direction:

$$\frac{\partial \Delta \sigma_{33}}{\partial \Delta e_{11}} = \frac{H_1(H_6 + H_7)mD}{1 - H_1(H_2 + H_3)} + nD$$

$$\frac{\partial \Delta \sigma_{33}}{\partial \Delta e_{22}} = \frac{H_1(H_6 + H_7)nD}{1 - H_1(H_2 + H_3)} + nD$$

$$\frac{\partial \Delta \sigma_{33}}{\partial \Delta e_{33}} = \frac{H_1(H_6 + H_7)nD}{1 - H_1(H_2 + H_3)} + mD$$

$$H_6 = (me_{33} - ne_L \xi_0)(D_m - D_a)(\xi_0^{\text{swit}} + \xi_t^{\text{swit}}) - nDe_L \xi_0^{\text{swit}}$$

$$H_7 = n(e_{11} + e_{22})(D_m - D_a)(\xi_0^{\text{swit}} + \xi_t^{\text{swit}}) \quad (\text{Eq 25})$$

Combining Eq 19, 23, 25 as well as the relations for the shear deformation, the Jacobian matrix can be summarized as*:

$$\frac{\partial \Delta \sigma}{\partial \Delta \varepsilon} = \begin{bmatrix} \frac{(\lambda+2\mu)}{H} & \frac{\lambda}{H} & \frac{\lambda}{H} & 0 & 0 & 0 \\ \frac{\tilde{H}}{H}(\lambda + 2\mu) + \lambda & \frac{\tilde{H}}{H}\lambda + (\lambda + 2\mu) & \frac{\tilde{H}}{H}\lambda + \lambda & 0 & 0 & 0 \\ \frac{\tilde{H}}{H}(\lambda + 2\mu) + \lambda & \frac{\tilde{H}}{H}\lambda + \lambda & \frac{\tilde{H}}{H}\lambda + (\lambda + 2\mu) & 0 & 0 & 0 \\ 0 & 0 & 0 & 2\mu & 0 & 0 \\ 0 & 0 & 0 & 0 & 2\mu & 0 \\ 0 & 0 & 0 & 0 & 0 & 2\mu \end{bmatrix} \quad (\text{Eq 26})$$

$$H = 1 - H_1(H_2 + H_3)$$

$$\tilde{H} = H_1(H_4 + H_5) \quad \text{except for zone [o, t]}$$

$$\tilde{\tilde{H}} = H_1(H_6 + H_7)$$

The general Jacobian matrix of this constitutive model can be derived by repeating this procedure for all transformation regions similar to that just derived for zone [A]. Only the result for these other regions is presented here. We refer interested readers to our previous article (Ref 2) for the linearization of the kinetics in the other transformation zones. If we consider the transformation kinetics in other zones except for the overlapping region [o, t], the Jacobian matrix has the same components as Eq 26 but with different expressions of H factors which should be revised as:

H_1 is given by Eq 17

$$H_2 = m(e_{11} - e_L \xi_0)(D_m - D_a)C_1^i - mDe_L C_{1s}^i$$

$$H_3 = n(e_{22} + e_{33})(D_m - D_a)C_1^i$$

$$H_4 = (me_{22} - ne_L \xi_0)(D_m - D_a)C_1^i - nDe_L C_{1s}^i \quad (\text{Eq 27})$$

$$H_5 = n(e_{11} + e_{33})(D_m - D_a)C_1^i$$

$$H_6 = (me_{33} - ne_L \xi_0)(D_m - D_a)C_1^i - nDe_L C_{1s}^i$$

$$H_7 = n(e_{11} + e_{22})(D_m - D_a)C_1^i$$

*It can be seen that the Jacobian matrix is not symmetric. Thus, the unsymmetric option must be used in ABAQUS.

Table 2 Parameters C_1^i and C_{1s}^i in the H factors for different zones allowing a unified matrix (Eq 26 and 27) in all cases excluding the overlapping [o, t] zone

Zone	C_1^i	C_{1s}^i
[A]	$\xi_0^{\text{swit}} + \xi_t^{\text{swit}}$	ξ_0^{swit}
[M][o]	$-(1 - \xi_0^{\text{swit}} - \xi_t^{\text{swit}})$	$-(1 - \xi_0^{\text{swit}})$
[t]	$-(1 - \xi_0^{\text{swit}} - \xi_t^{\text{swit}})$	0
[o, t]	see Eq 28 and 29	

C_1^i and C_{1s}^i refer to Table 2.

For the overlapping region [o, t], the transformation kinetics developed recently (Ref 2) is applied and the Jacobian matrix is obtained, which has the same expression as Eq 26 but with different H factors:

$$H = 1 - H_1^s(H_2^s + H_3^s) - H_1^t(H_2^t + H_3^t)$$

$$\tilde{H} = H_1^s(H_4^s + H_5^s) + H_1^t(H_4^t + H_5^t) \quad (\text{Eq 28})$$

$$\tilde{\tilde{H}} = H_1^s(H_6^s + H_7^s) + H_1^t(H_6^t + H_7^t)$$

$$H_1^i = \sin(\pi Z^i) \cdot \frac{-\frac{1}{2} \pi n_2^i}{n_1^i(T_{\text{out}}^i - T_j^i) + n_2^i(\sigma_{\text{out}}^i - \sigma_j^i)}$$

$$H_2^i = m(e_{11} - e_L \xi_0)(D_m - D_a)C_{1\text{mix}}^i - m\varepsilon_L DC_{1\text{smix}}^i$$

$$H_3^i = n(e_{22} + e_{33})(D_m - D_a)C_{1\text{mix}}^i$$

$$H_4^i = (me_{22} - ne_L \xi_0)(D_m - D_a)C_{1\text{mix}}^i - nDe_L C_{1\text{smix}}^i$$

$$H_5^i = n(e_{11} + e_{33})(D_m - D_a)C_{1\text{mix}}^i$$

$$H_6^i = (me_{33} - ne_L \xi_0)(D_m - D_a)C_{1\text{mix}}^i - nDe_L C_{1\text{smix}}^i$$

$$H_7^i = n(e_{11} + e_{22})(D_m - D_a)C_{1\text{mix}}^i$$

$$i = o, t \quad (\text{Eq 29})$$

where

$$C_{1\text{mix}}^s = -(1 - \xi_t^{\text{swit}} - \xi_0^{\text{swit}})f^A(Z^t)$$

$$C_{1\text{smix}}^s = (\xi_s^{\text{swit}} - 1)$$

$$C_{1\text{mix}}^t = -(1 - \xi_t^{\text{swit}} - \xi_0^{\text{swit}})f^A(Z^o)$$

$$C_{1\text{smix}}^t = 0$$

For other regions where no change in martensite fraction occurs, the Jacobian matrix reduces to the standard constitutive relations for the isotropic material, which is

$$\frac{\partial \Delta \sigma}{\partial \Delta \varepsilon} = \begin{bmatrix} (\lambda + 2\mu) & \lambda & \lambda & 0 & 0 & 0 \\ \lambda & (\lambda + 2\mu) & \lambda & 0 & 0 & 0 \\ \lambda & \lambda & (\lambda + 2\mu) & 0 & 0 & 0 \\ 0 & 0 & 0 & 2\mu & 0 & 0 \\ 0 & 0 & 0 & 0 & 2\mu & 0 \\ 0 & 0 & 0 & 0 & 0 & 2\mu \end{bmatrix} \quad (\text{Eq 30})$$

3.2 Model Implementation in ABAQUS

After obtaining the Jacobian matrix for all regions in the phase diagram, this SMA model is implemented into ABAQUS via its UMAT interface. The iteration procedure is described briefly in the following:

1. At the beginning of the increment, all field variables, including current strain, strain increment, current temperature, temperature increment, etc., are passed into the user subroutine.
2. A similar iteration strategy to that in Ref 2 is employed to calculate the stress field based on the strain and temperature input. If a convergent result is not obtained in this step, the current iteration is stopped and the time step decreases. This process will continue until either the convergent solution is obtained or the maximum allowable number of trials is exceeded.
3. After convergent stresses are obtained, the H factors as well as the tangent matrix $\frac{\partial \Delta \sigma}{\partial \Delta \epsilon}$ are calculated in the subroutine and provided to ABAQUS. Other field variables like switching points, convergent points are also updated for the next calculation. For the detailed updating strategy, please refer to the previous article (Ref 2).

3.3 Two-Way Shape Memory Effect (TWSME)

The two-way shape memory effect is another common property of shape memory alloys, which usually occurs as the result of thermo-mechanical training applied to materials. Unlike the one-way material, the two-way SMAs are able to “remember” a geometrical shape at a higher temperature and another shape at a lower temperature through a mechanism of residual microscopic strains in the martensite phase of the material. This unique effect enables SMAs to be used in many applications, like reversible fasteners, medical implants, etc. (Ref 14). The two-way shape memory effect needs to be taken into account in our finite element implementation because the SMA wires used in the test exhibit strong two-way behavior.

Although the constitutive law adopted here is intended to deal with one-way shape memory effect, we can alter the model to allow the ability to capture the essential behavior of the TWSME. As already pointed by Amengual et al. (Ref 15), the training process tends to shift the phase diagram lower. Prahlad and Chopra (Ref 16) characterized the critical stress-temperature diagram for SMA wire via a series of experimental tests and found that the σ_{cr}^s decreases to zero at low temperature. Moreover, recent studies by Peultier et al. (Ref 17) and Wu et al. (Ref 18) show the transformation strain is very sensitive to the stress at low stress level. Combined those observations, we propose a modified phase diagram here to address the two-way effect but without losing the generality of our implementation. In the new phase diagram (Fig. 3), the critical stress σ_{cr}^f can be determined experimentally as the stress when a saturation of transformation strain occurs, while the other critical stresses σ_{cr}^s becomes an adjustable parameter that are allowable to change along the stress axis even to the negative region. When the σ_{cr}^s is set to zero or a negative value, the martensite phase is self-oriented even at low stress level in contrast to only self-accommodated martensite at low stress in the original phase diagram. In this manner, the transformation strain is nonzero when the temperature decreases at the constant stress and the magnitude of the two-way strain depends on the relative

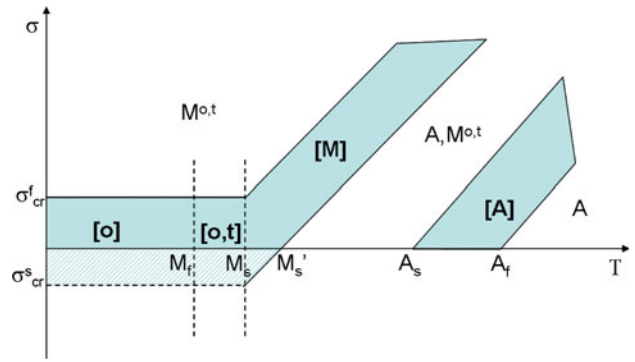


Fig. 3 The modified phase diagram that the lower bound of [o] and [o, t] zones are shifted to the compressive side. With the aid of this diagram, the original model can be used to simulate TWSME

position of the applied stress inside of the region [o, t]. Note that the definition of the transformation temperatures is slightly different from the original diagram because we shift the region [t] and part of regions [o], [o, t] into the compressive regime. Thus, the intersecting point, M_s' , between zone [M] and temperature axis becomes a new transformation temperature that the parent phase starts to transform to the martensite phase when the temperature is lower than M_s' .

Figure 4 shows an example of the TWSME simulation where the material properties were extracted from the literature (Ref 19) and the result was also compared with their experiment. From this figure, it was clear that by setting the σ_{cr}^s to a value lower than zero, -130 Mpa in this case, this model could be used to simulate the TWSME.

4. Finite Element Simulation of the Seal

An axisymmetric finite element model was created to represent the working scenario of the lip seal mounting on a shaft (see Fig. 1). Herein, the shaft was modeled as a rigid surface due to its high stiffness in comparison with other components and the garter spring was modeled as an annulus to reflect the hollow property of the real spring. To study the effect of SMAs on the seal, an SMA ribbon was placed inside of the garter spring, consistent with configuration of the prototype of the SMA enhanced seal (Ref 1). SMA ribbon instead of wire was used to simplify modeling since circular section of a wire requires much more elements to represent the geometry. Three pairs of contacts were defined in this model to simulate the interaction between components, which were shaft versus seal, seal versus spring, and spring versus SMA ribbon.

The seal used in this application was made of poly(tetrafluoroethylene) (PTFE) which is a type of semi-crystalline polymer and has a very complex visco-plastic material behavior. Due to insufficient experimental data of the seal material, we used material properties of PTFE material published in literatures for the simulation. Since it was to demonstrate the enhancement of sealing performance caused by the SMA wire, in this study, we only considered the elastic behavior of the PTFE seal to simplify the calculation without losing the generality of the method. Note that material properties of PTFE in compression are not the same as that in tension. Considering the seal is mostly under compression, the PTFE material parameters measured in compressive

condition was adopted as the seal properties in this study. The temperature-dependent material properties of PTFE are summarized in Table 3.

The garter spring is a coil spring and was modeled as a solid annulus to reflect the hollow property of the real spring. The Young's modulus of spring element in the axial direction was estimated based on the force-deflection curve of a standard axial spring, which was about 550 MPa. Other material parameters were not so important that some values within the reasonable range were assigned to fill the stiffness matrix. Herein, an isotropic behavior was assumed for the spring with $E = 500$ MPa and $\nu = 0.3$.

It was more of challenge to obtain the material properties of the SMA wire since it requires at least 15 parameters to fully describe the material behavior of SMAs in the pseudo 3D model. In Table 4, we list data collected for this type of wires

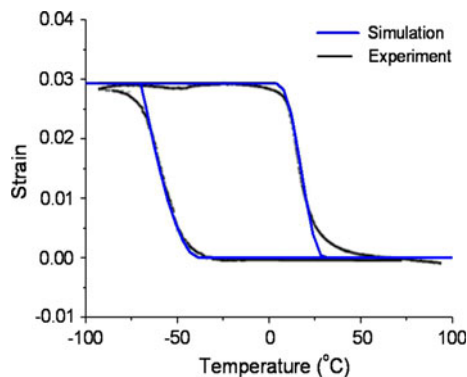


Fig. 4 Comparison of TWSME at zero stress computed by the UMAT and experiment results. The parameters used for the simulation are: $A_f = 30$ °C, $A_s = 5$ °C, $M_s' = -45$ °C, $M_f = -75$ °C, $\varepsilon_L = 7\%$, $\sigma_{cr}^s = -130$ MPa, and $\sigma_{cr}^f = 160$ MPa (Ref 19)

Table 3 The material properties of Teflon in compression (data from Ref 20)

Temperature, °C	E , GPa
-200	1.6
-100	1.5
0	0.8
24	0.5
50	0.267
100	0.117
150	0.088

Table 4 Material properties of SMA wires used in this simulation

$E_a = 67$ GPa (a)	$A_f = 83.4$ °C (c)	$C_a = 8.37$ MPa/°C (c)	$\varepsilon_L = 6.7\%$ (c)
$E_m = 26.7$ GPa (a)	$A_s = 67$ °C (c)	$C_M = 7.78$ MPa/°C (c)	$\varepsilon_{TW} = 1.7\%$ (c)
$\nu_a = 0.45$ (b)	$M_s = 50.5$ °C (c)	$s_{scr} = -32$ MPa (d)	$a = 0$ (b)
$\nu_m = 0.45$ (b)	$M_f = 36.5$ °C (c)	$s_{fcr} = 48$ MPa (d)	

(a) Typical Young's moduli for NiTi SMA wire

(b) Assumptions in this article

(c) Typical values for the 90 °C Dynalloy Flexinol SMA wire

(d) Derived based on TWSME and typical NiTi Properties

from different sources as well as some assumptions of the material.

The initial oriented martensite fraction in the SMA wire was set to 0.2 with respect to the 1.4% two-way strain at low temperature, while the initial self-accommodated martensite fraction was 0.8. In order to simulate the SMA enhancement on the sealing performance, two thermal steps was applied to the model. In the first step, the temperature was ramped up from 25 to 140 °C which is the highest possible temperature required for the seal application described in the experimental counterpart. Followed was a cooling step to 25 °C. Calculations were performed in ABAQUS standard and the average contact pressure between the rod and the seal was plotted (Fig. 5).

In Fig. 5, the pressure response can be easily divided into following stages: the first step was the initial shrink fit such that the pressure increased until reaching equilibrium. The model was then heated up, resulting in a decrease of the contact pressure due to softening of the seal material. This trend stopped when the temperature was about 70 °C, because the reverse phase transformation from martensite to austenite occurs in the SMA wire. The restrained recovery force induced by the SMA wire caused the increase of pressure between seal and the shaft. In the third step, the model was cooled back to room temperature. Initially, the contact pressure slightly increases due to the seal material hardening and then followed by a drop of pressure because of the phase transformation from austenite to martensite. The pressure resumed increasing after the phase transformation finished. The loading path of the SMA wire overlaid on the phase diagram was shown in Fig. 6 to better illustrate the start point of phase transformation in the SMA wire.

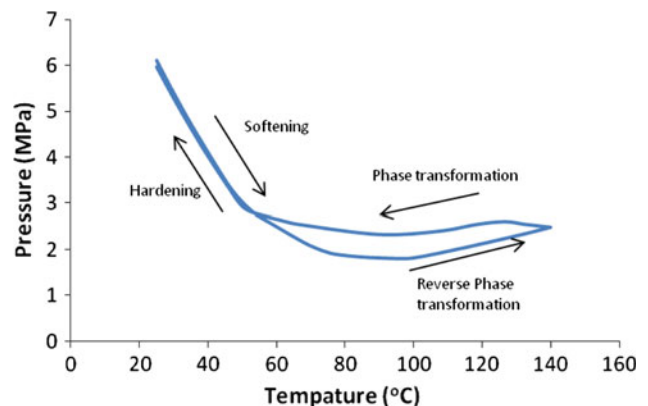


Fig. 5 Average contact pressure versus temperature for the model with 1.4% prestrain

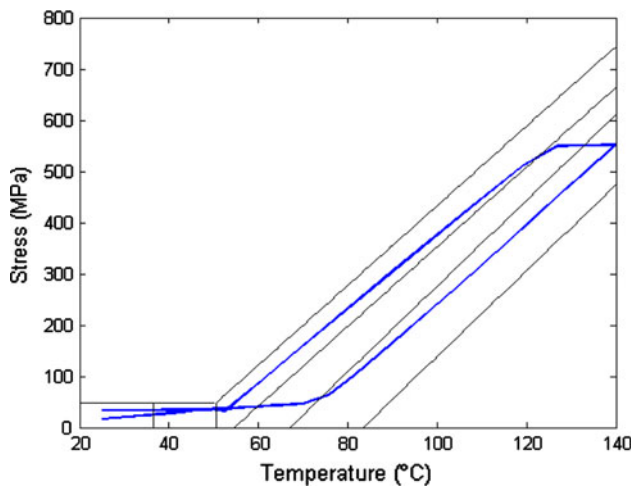


Fig. 6 Loading path of the SMA wire overlaid on the phase diagram

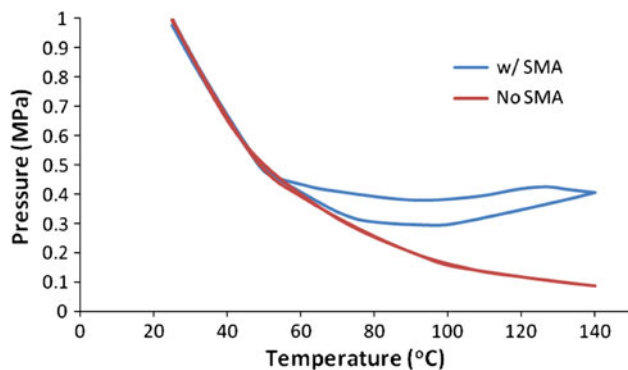


Fig. 7 Comparison of the normalized contact pressure for two seals: With SMA wire and without SMA wire

In order to better understand the influence of the SMA wire, the sealing performance of the same seal without an SMA wire was simulated with the exactly same loading steps. The predicted contact pressures on the shaft for both models were normalized and plotted in one figure to give a better comparison (Fig. 7). It is clear that the SMA wire reduced the variation of the contact pressure during the thermal cycle: maximum 70% decrease of the contact pressure for the SMA enhanced seal in comparison with 90% decrease for the normal seal without SMA wire. Particularly, the restrained recovery force by the SMA wire countered the effect of seal material softening at high temperature, which could potentially reduce the leaking issue of lip seals noticed in the application.

The simulation results qualitatively agreed with the experimental observation presented in the experimental counterpart (Ref 1): For the setup with a normal lip seal, the leakage rate was proportional to the temperature, indicating the lower sealing performance of the seal due to material softening and thermal expansion. By contrast, the leakage rate no longer linearly correlated to the temperature after adding the SMA wire into the seal and the overall fluctuation was much smaller compared to the system with a normal seal. The leakage rate even decreased when the temperature changed from 80 to 100 °C, which could be attributed to the SMA wire enhancing the sealing pressure as temperature increases.

5. Conclusion

In this study, we presented a finite element model to simulate the sealing performance of an SMA enhanced seal under a thermal loading cycle. A pseudo-3D constitutive model was proposed to better capture the thermo-mechanical responses of wire-shape SMA components. In this model, the one-dimensional constitutive law for shape memory alloys developed by Brinson (Ref 3) was used to characterize the thermo-mechanical behaviors related to SMAs in the axial direction, and the linear elastic response was assumed in the other directions. This approach enables the model to capture simple spatial responses without losing the advantages of the unified one-dimensional constitutive law that are simple, robust, and low computational cost. The model was then implemented into ABAQUS using the user-defined material subroutine (UMAT) that inherits most features of the commercial finite element package including support for most continuum elements, contact analysis, compatibility with ABAQUS CAE, etc. Two-way shape memory effect was considered in this model by shifting existing phase diagram since the SMA wire used for the protocol exhibits strong two-way effect.

An axisymmetric model was created to simulate the working environment of a lip seal that was mounted on a shaft rod. In order to better understand the effect of the SMA wire, the performance of a seal with and without the SMA wire was simulated with the same parameters. Due to insufficient material properties and measurement techniques, direct comparison between the simulation and the experiment on the sealing pressure was not possible for this study. However, the qualitative agreement with the experimental observation verified the SMA model and its versatility for predicting thermo-mechanical behavior of structures with wire-shape SMA components. The simulation presented in this study was just an example of the application of this SMA model. With the capability of the FEA package, ABAQUS, it can be a very powerful and useful tool in the design, validation, and optimization of SMA devices in which SMAs mainly exhibit one-dimensional behavior.

References

1. X. Gao, R. Qiao et al., Experimental Setup and Results of an SMA Enhanced Lip Seal, *J. Intell. Mater. Syst. Struct.*, 2011 (to be submitted)
2. X. Gao, R. Qiao, and L.C. Brinson, Phase Diagram Kinetics for Shape Memory Alloys: A Robust Finite Element Implementation, *Smart Mater. Struct.*, 2007, **16**, p 2102–2115
3. L.C. Brinson, One Dimensional Constitutive Behavior of Shape Memory Alloys: Thermomechanical derivation with non-constant material functions, *J. Intell. Mater. Syst. Struct.*, 1993, **4**(2), p 229–242
4. L.C. Brinson and M.S. Huang, Simplifications and Comparisons Of Shape Memory Alloy Constitutive Models, *J. Intell. Mater. Syst. Struct.*, 1996, **7**(1), p 108–114
5. M.A. Qidwai and D.C. Lagoudas, Numerical Implementation of a Shape Memory Alloy Thermomechanical Constitutive Model Using Return Mapping Algorithms, *Int. J. Numer. Methods Eng.*, 2000, **47**, p 1123–1168
6. J.G. Boyd and D.C. Lagoudas, A Thermodynamical Constitutive Model For Shape Memory Materials. 1. The Monolithic Shape Memory Alloy, *Int. J. Plast.*, 1996, **12**(6), p 805–842
7. A. Bekker and L.C. Brinson, Phase Diagram Based Description of the Hysteresis Behavior of Shape Memory Alloys, *Acta Mater.*, 1998, **46**(10), p 3649–3665

8. K. Tanaka, A Thermomechanical Sketch of Shape Memory Effect—One-Dimensional Tensile Behavior, *Res. Mech.*, 1986, **18**(3), p 251–263
9. Y. Ivshin and T.J. Pence, A Constitutive Model for Hysteretic Phase-Transition Behavior, *Int. J. Eng. Sci.*, 1994, **32**(4), p 681–704
10. C. Segui, E. Cesari, and J. Pons, Phenomenological Modeling of the Hysteresis Loop in Thermoelastic Martensitic Transformations, *Mater. Trans. JIM*, 1992, **33**(7), p 650–658
11. C. Liang and C.A. Rogers, One-Dimensional Thermomechanical Constitutive Relations for Shape Memory Materials, *J. Intell. Mater. Syst. Struct.*, 1990, **1**(2), p 207–234
12. Q.P. Sun and K.C. Hwang, Micromechanics Modeling for the Constitutive Behavior of Polycrystalline Shape Memory Alloys. 1 Derivation of General Relations, *J. Mech. Phys. Solids*, 1993, **41**(1), p 1–17
13. E. Patoor, M.E. Amrani, A. Eberhardt, and M. Berveiller, Determination of the Origin for Dissymmetry Observed Between Tensile and Compression Tests on Shape Memory Alloys, *III European Symposium on Martensitic Transformations: ESOMAT'94*, Barcelona, Spain, J. Phys. IV, Colloq. (France), Vol 5, no C2, A. Planes, J. Ortín, and L. Mañosa, Eds., Editions de Physique, Les Ulis, France, 1995, p 495–500
14. F. Auricchio, S. Marfia, and E. Sacco, Modeling of SMA Materials: Training and Two Way Memory Effects, *Comput. Struct.*, 2003, **81** (24–25), p 2301–2317
15. A. Amengual, E. Cesari, and R. Romero, On the Relationship Between Temperature and Critical Stress in the 2-Way Shape-Memory Effect of Cu-Zn-Al Single-Crystals, *Scripta Metall. Mater.*, 1995, **32**(8), p 1269–1275
16. H. Prahlad and I. Chopra, Experimental Characterization of Ni-Ti Shape Memory Alloy Wires Under Uniaxial Loading Conditions, *J. Intell. Mater. Syst. Struct.*, 2000, **11**(4), p 272–282
17. B. Peultier, T. Ben Zineb, and E. Patoor, Macroscopic Constitutive Law of Shape Memory Alloy Thermomechanical Behaviour. Application to Structure Computation by FEM, *Mech. Mater.*, 2006, **38**(5–6), p 510–524
18. X.D. Wu, G.J. Sun, and J.S. Wu, The Nonlinear Relationship Between Transformation Strain and Applied Stress for Nitinol, *Mater. Lett.*, 2003, **57**(7), p 1334–1338
19. R. Lahoz and J.A. Puertolas, Training and Two-Way Shape Memory in NiTi Alloys: Influence on Thermal Parameters, *J. Alloys Compd.*, 2004, **381**(1–2), p 130–136
20. P. Rae and D. Dattelbaum, The Properties of poly(tetrafluoroethylene) (PTFE) in Compression, *Polymer*, 2004, **45**, p 7615–7625